

Peptides in Presence of Aqueous Ionic Liquids: Tunable Co-Solutes as Denaturants or Protectants? -Supplementary Material-

Volker Lesch,[†] Andreas Heuer,[†] Vasileios A. Tatsis,[†] Christian Holm,[‡] and Jens
Smiatek^{*,‡}

*Institut für Physikalische Chemie, Westfälische Wilhelms-Universität Münster, D-48149
Münster, Germany, and Institut für Computerphysik, Universität Stuttgart, D-70569
Stuttgart, Germany*

E-mail: smiatek@icp.uni-stuttgart.de

*To whom correspondence should be addressed

[†]Institut für Physikalische Chemie, Westfälische Wilhelms-Universität Münster, D-48149 Münster, Germany

[‡]Institut für Computerphysik, Universität Stuttgart, D-70569 Stuttgart, Germany

General simulation details

The molecular dynamics simulations have been performed with the software package GRO-MACS (version 4.6.7)^{1,2} utilizing the non-polarizable CL&P force field for EMIM and ACE³⁻⁶, the OPLS/AA force field for the peptide⁷, which is compatible with the CL&P force field³ and the TIP3P water model for the aqueous solution⁸. The number of EMIM ACE pairs was $N_{pairs} = 250$ which results in an effective concentration of $c = 0.57$ mol/L in the NpT simulations. Periodic boundary conditions were applied in each direction of a cubic box with a box length of 9 nm. The initial structure of the protein was downloaded from *www.pdb.org*, identifier 2GB1⁹ with the residues 41-56. The negative charge of the peptide was compensated by adding the corresponding number of sodium ions. The electrostatic interactions were calculated via the smooth Particle-Mesh-Ewald method^{10,11} with a cutoff range of 1.2 nm and an accuracy of 10^{-6} . For energy minimization, we used the conjugate gradient method with an energy tolerance value of 100 kJ/mol/nm and a step size of 10^{-4} nm. The time step in all simulations was 1 fs. For the NVT and the NpT simulations, we used the Nose-Hoover thermostat¹² with a coupling time of 1 ps and the Parrinello-Rahman barostat¹³ with a coupling time of 2 ps, a reference pressure of 1 bar and a compressibility of 4.5×10^{-10} Pa⁻¹.

High temperature simulations

After energy minimization of the initial structure and an equilibration run of 20 ns with position restraints for the energy-minimized peptide state, high temperature simulations ($T = 500$ K) in pure water were conducted in order to identify appropriate collective variables and to obtain reliable conformations. The simulation length was 100 ns in a NVT ensemble. The temperature was controlled by a Nose-Hoover thermostat.

Restrained simulations

The folded and unfolded structures were extracted from the high temperature simulation. These structures were dissolved in pure water and ionic liquid/water mixtures using a box length of 9 nm. The folded and unfolded structures were restrained with respect of the heavy C_α atoms to study the accumulation of water and IL around the peptide. All simulations were performed in a NpT ensemble. First, the systems were simulated for 100 ns at $T = 500$ K to achieve a well mixed system. After these simulations, the temperature was decreased to $T = 298$ K for a 100 ns production run where the first 10 ns were discarded for the analysis. The elementary integration step for all simulations was 1 fs.

Metadynamics simulations

The initial configuration for the metadynamics simulations was the energy-minimized solvated structure of the residues 41-56 of peptide 2GB1. We performed an equilibration run of 20 ns with position restraints. Hereafter, the position restraints were released in the Metadynamics simulations. The metadynamics simulations were performed using PLUMED 2.1.1¹⁴. The end-to-end distance (R_e) and the root mean-square deviation (RMSD) were used as collective variables where $RMSD = 0$ nm corresponds to the energy-minimized reference state. The height of the hills was 0.1 kJ, the width was given by 0.1 nm and a new hill was deposited after 1 ps¹⁵. Convergence of the free energy landscapes was checked with regard to the motion in the collective variable phase space such that two complete cycles of folding and unfolding motion have been performed. The simulations were performed in a NVT ensemble at 298 K.

Properties of conservative interactions

In order to evaluate the interactions that mainly drive the unfolding of the native conformation, we have calculated the electrostatic Coulomb and the Lennard-Jones interaction

energies between EMIM and ACE and the folded and the unfolded peptide conformation. The results are presented in Fig. 1. With regard to the results for the folded conforma-

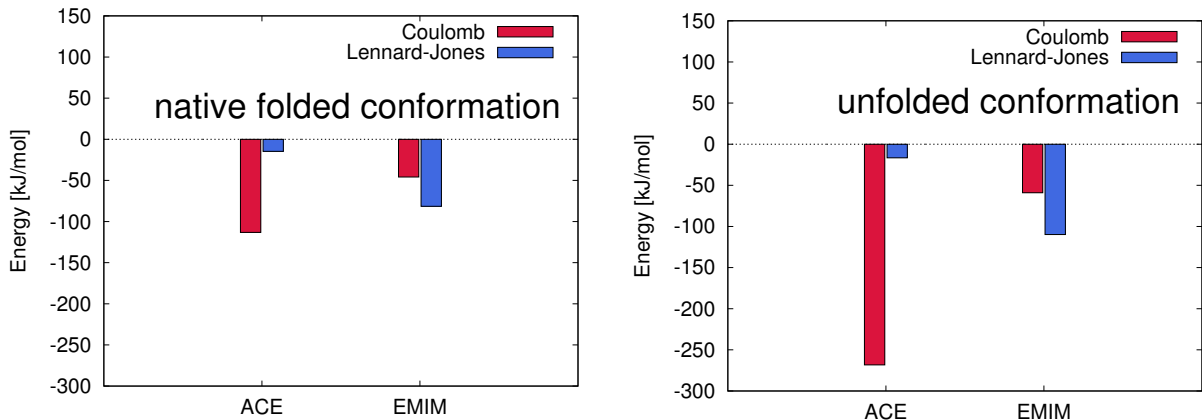


Figure 1: Left: Coulomb (red bars) and Lennard-Jones energies (blue bars) between the folded 2GB1 conformation and EMIM and ACE. Right: Coulomb (red bars) and Lennard-Jones energies (blue bars) between the unfolded 2GB1 conformation and EMIM and ACE.

tion, it can be clearly seen that ACE ions mostly interact via electrostatic interactions with the peptide. Lennard-Jones interactions are less pronounced in contrast to the interactions between the peptide and EMIM. A nearly identical EMIM behavior can be found for the unfolded conformation. The most pronounced difference compared with the folded conformations is given by the strong increase of the net electrostatic energy between ACE and the peptide. This finding is in good agreement to the results obtained for the preferential binding coefficients in the main article where it can be seen that ACE reveals a significant structure-dependent binding to the peptide. The results shown here indicate that this binding is mainly induced by stronger electrostatic interactions in presence of the unfolded conformation. The details of the unfolding mechanism will be discussed in the next section. In summary, the smaller ACE anions mostly interact via electrostatic interactions with the peptide while the EMIM-peptide interactions are dominated by Lennard-Jones interactions due to the bulky character of the EMIM cation.

We have also evaluated the energetic contributions between the peptide and the ethyl- and methylgroups of EMIM and ACE. The corresponding results are presented in Fig. 2. It be-

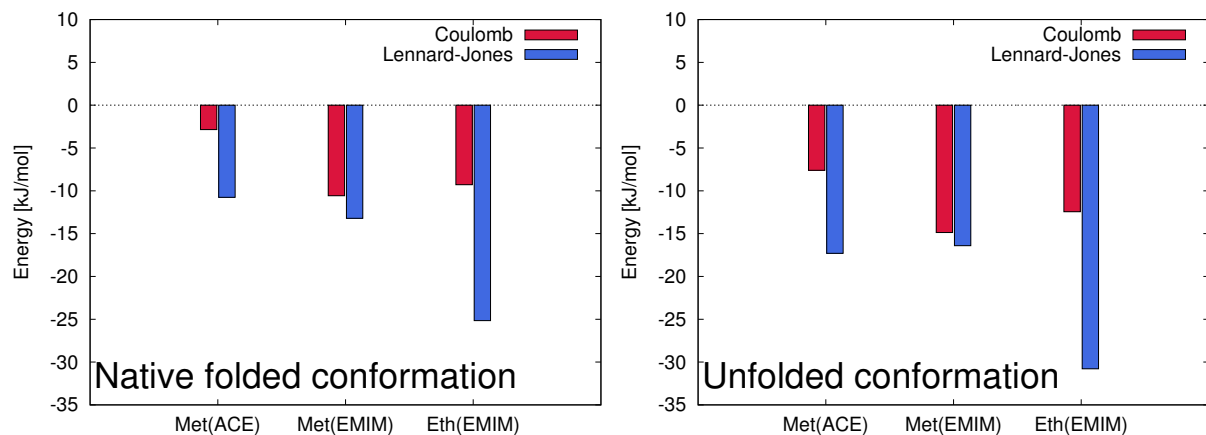


Figure 2: Left: Coulomb (red bars) and Lennard-Jones energies (blue bars) between the folded hairpin conformation and the methyl group of ACE (Met(ACE)), the methylgroup of EMIM (Met(EMIM)) and the ethylgroup of EMIM (Eth(EMIM)). Right: Coulomb and Lennard-Jones energies between the unfolded conformation of the peptide and the methyl group of ACE (Met(ACE)), the methylgroup of EMIM (Met(EMIM)) and the ethylgroup of EMIM (Eth(EMIM)).

comes obvious that the ethyl- and the methylgroup of EMIM strongly contribute to the total Lennard-Jones energies shown in Fig. 1. Moreover, also pronounced Coulomb interactions induced by the partial charges of the atoms can be observed. However, the energetic differences between the folded and the unfolded conformation are more or less marginal for the ethyl- and the methylgroup of EMIM. Hence, it can be seen that the unspecific Lennard-Jones binding energy between the peptide and EMIM can be mostly attributed to the presence of the alkylgroups.

In contrast, the influence of the methylgroup in ACE is less pronounced. The Lennard-Jones interaction energies are less significant compared with the overall binding energies and can be mostly neglected. Therefore it can be concluded that the presence of the alkylgroups in EMIM results in an unspecific binding behavior to the peptide whereas the strong accumulation of ACE shown in the next section is mostly driven by electrostatic interactions as induced by the carboxylgroup.

Preferential binding coefficients for EMIM and ACE with the single peptide residues

In order to detect a binding of EMIM or ACE to specific amino acids, we have calculated the preferential binding coefficients between ACE and EMIM and all residues of the peptide. The cut-off radius for the evaluation of the Kirkwood-Buff integrals was $r_c = 3.0$ nm. The results are presented in Fig. 3. It can be clearly seen that EMIM shows a strong preferential

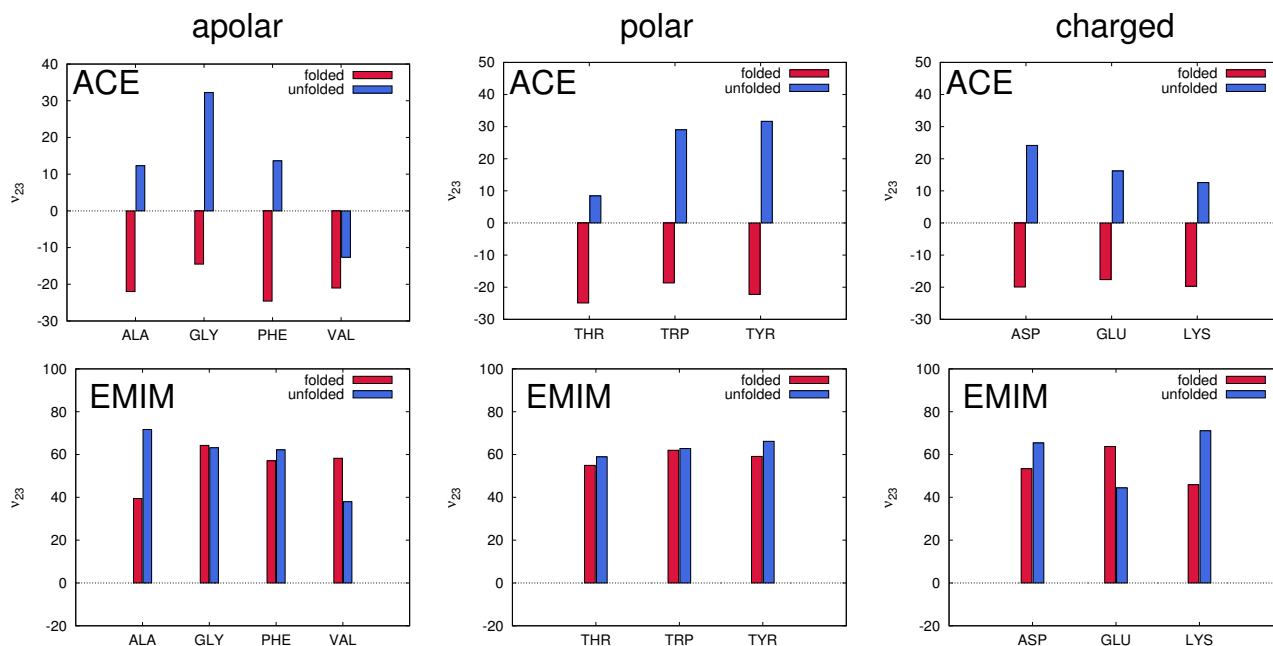


Figure 3: Top row: Preferential binding coefficients ν_{23} between ACE and all apolar amino acids (left column), all polar amino acids (middle column) and all charged amino acids (right column). The blue bars denote the preferential binding coefficient for the folded 2GB1 conformation whereas the red bars denote the values for the unfolded 2GB1 state. The data for the EMIM preferential binding coefficients are presented in the bottom row.

binding to all amino acids, regardless of their apolar, polar or charged properties. Slight differences for the EMIM related preferential binding coefficients between the folded and the unfolded 2GB1 conformation are only given for the amino acids ALA, VAL and all charged residues. Indeed, this more or less unspecific binding behavior can be related to the strong dominance of Lennard-Jones interactions due to the bulky properties of EMIM which is

validated by the results shown in Fig. 1. We will see below that EMIM mostly occupies the position in the first solvent shell such that short-ranged Lennard-Jones interactions are favorable.

In contrast, ACE shows a distinct binding behavior to the folded and the unfolded conformation. Thus, a preferential exclusion ($\nu_{23}^f < 0$) of ACE can be found around all amino acids of the folded conformation whereas a preferential binding behavior ($\nu_{23}^u > 0$) is evident for the binding of acetate ions to nearly all amino acids of the unfolded conformation. The only preferential exclusion behavior of ACE around the unfolded conformation can be recognized for VAL. This behavior can be explained by a diminished accessible space around VAL for the unfolded conformation which is also obvious in combination with the smaller EMIM preferential binding coefficient values. The strongest differences between the ACE preferential binding coefficients to the folded and the unfolded conformation can be found for GLY, TRP, TYR and ASP. Indeed, ASP is likewise charged as ACE such that the occurrence of attraction as induced by the preferential binding coefficients is more or less counter-intuitive. We will discuss below the corresponding mechanism which leads to this surprising behavior. In summary, it becomes clearly evident that the structure specific preferential binding of ACE as induced by electrostatic interactions represents the main driving force for the unfolding of the peptide.

Radial distribution function between specific amino acids and EMIM/ACE for the folded and the unfolded conformation

In the previous section, it has been discussed that ACE is strongly attracted to nearly all amino acids of the unfolded 2GB1 conformation. With regard to the underlying radial distribution functions, a detailed explanation of this effect can be given which is also a

prerequisite for the understanding of the full unfolding mechanism. The corresponding radial distribution functions between EMIM and ACE and the amino acids GLY, TYR and ASP with regard to the folded and the unfolded 2GB1 conformation are shown in Fig. 4. The amino acids were chosen with respect to the largest differences found for the ACE preferential binding coefficients to the folded and the unfolded conformation for polar, apolar and charged species. It can be clearly seen that EMIM cations are located in the first solvent shell

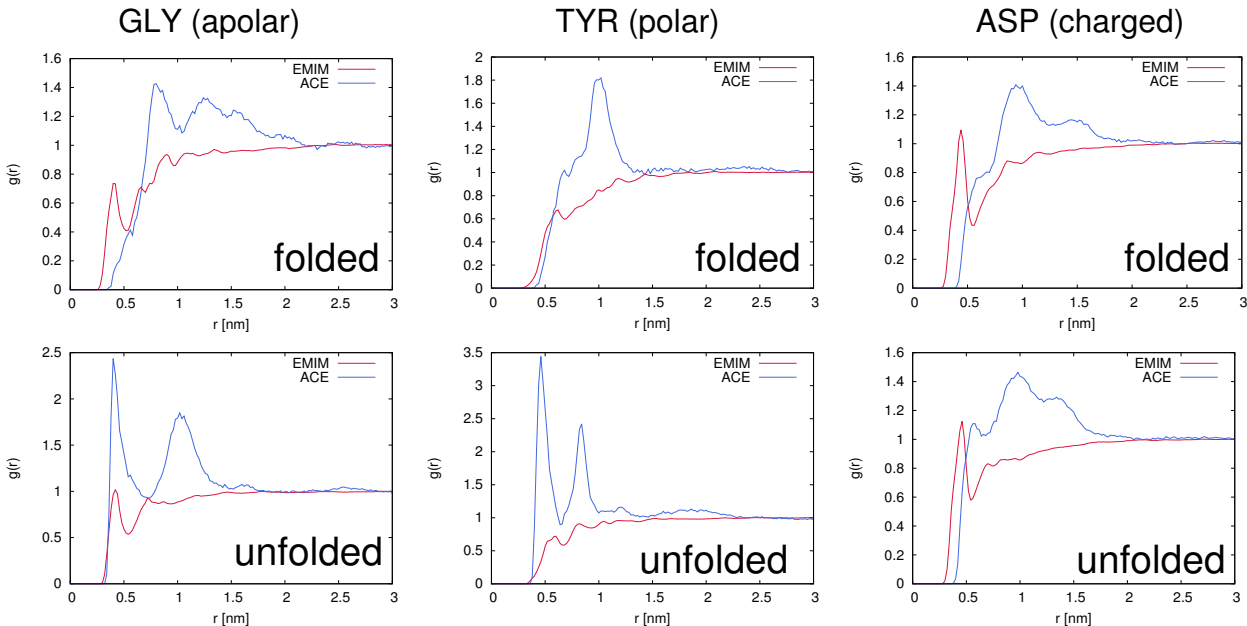


Figure 4: Top row: Radial distribution functions between ACE (blue line) or EMIM (red line) and the apolar amino acid GLY (left column), the polar amino acid TYR (middle column) and the charged amino acid ASP (right column) for the folded 2GB1 conformation. The corresponding radial distribution functions for the unfolded 2GB1 conformation are shown in the bottom row. All radial distribution functions have been calculated with regard to the center-of-mass of the corresponding groups.

($r \leq 0.5$ nm) around all the considered amino acids. This observation can be explained with regard to the dominance of Lennard-Jones interactions between the peptide and the EMIM cations. Hence, electrostatic interactions are minor important such that an unspecific binding behavior can be observed which explains the strong accumulation of EMIM ions around all amino acids.

Indeed, the ACE anions form the second solvent shell around all amino acids for the folded

conformation with a distance of $r \geq 0.5$ nm. Thus, the first solvent shell is fully occupied by the bulky EMIM cations such that a shorter distance of ACE to the peptide is not realizable due to excluded volume effects. Indeed, the positive charge of the EMIM cations also strongly attracts the ACE anions. This specific behavior has been also observed and discussed in a recent publication in terms of the accumulation behavior for EMIM and ACE ions around model spheres¹⁶. The position of ACE in the second solvent shell around the folded conformation can be interpreted as a preferential exclusion behavior as induced by the EMIM cations with regard to the corresponding preferential binding coefficients.

Indeed, if the peptide unfolds, the accessible space around the unfolded conformation is less confined such that ACE anions might also occupy the first solvent shell to form more stable EMIM-ACE ion pairs. This ACE behavior can be easily recognized in Fig. 4 for all radial distribution functions with regard to the unfolded conformation where the ACE radial distribution function peak values significantly increase at distances $r \leq 0.5$ nm. The strong ACE accumulation around the unfolded conformation at short distances is induced by the positive charge of EMIM and favored by the larger accessible solvent area of the peptide. This effect is even evident for the negatively charged amino acid ASP as can be seen by the results in Fig. 4 although the position of the first ACE shell around the unfolded conformation is slightly shifted to larger distances due to electrostatic repulsion. Thus, the accumulation of ACE anions in the first EMIM layer is mainly induced by the formation of ACE-EMIM ion pairs and can be interpreted as a structure dependent preferential binding which induces an unfolding of the peptide.

Explanation of the unfolding mechanism

A prerequisite of the observed effects is given by the presence of a bulky cation or anion that strongly interacts via Lennard-Jones interactions with the peptide. The smaller co-ion accumulates in the second layer around the folded conformation of the peptide due to strong

electrostatic interactions with the cation. Indeed, the formation of energetically favorable EMIM-ACE ion pairs in the first layer around the hairpin is finally accomplished by the unfolding of the peptide which results in a larger solvent-accessible surface area. Hence, the preferential binding of ACE to the unfolded conformation to compensate the charge of the EMIM layer can be therefore interpreted as the main mechanism which biases the unfolding of the hairpin conformation. Indeed, this mechanism is strongly specific for ionic liquids due to the presence of two oppositely charged ion species.

References

- (1) van der Spoel, D.; Lindahl, E.; Hess, B.; Groenhof, G.; Mark, A. E.; Berendsen, H. J. C. GROMACS: Fast, flexible, and free. *J. Comput. Chem.* **2005**, *26*, 1701–1718.
- (2) Pronk, S.; Páll, S.; Schulz, R.; Larsson, P.; Bjelkmar, P.; Apostolov, R.; Shirts, M. R.; Smith, J. C.; Kasson, P. M.; van der Spoel, D.; Hess, B.; Lindahl, E. GROMACS 4.5: a high-throughput and highly parallel open source molecular simulation toolkit. *Bioinformatics* **2013**, *29*, 845–854.
- (3) Canongia Lopes, J. N.; Deschamps, J.; Padua, A. A. H. Modeling ionic liquids using a systematic all-atom force field. *J. Phys. Chem. B* **2004**, *108*, 2038–2047.
- (4) Canongia Lopes, J. N.; Padua, A. A. H. Molecular force field for ionic liquids III: imidazolium, pyridinium, and phosphonium cations; chloride, bromide, and dicyanamide anions. *J. Phys. Chem. B* **2006**, *110*, 19586–19592.
- (5) Canongia Lopes, J. N.; Padua, A. A. H. Molecular force field for ionic liquids composed of triflate or bistriflylimide anions. *J. Phys. Chem. B* **2004**, *108*, 16893–16898.
- (6) Canongia Lopes, J. N.; Padua, A. A. H.; Shimizu, K. Molecular force field for ionic liquids IV: trialkylimidazolium and alkoxycarbonyl-imidazolium cations; alkylsulfonate and alkylsulfate anions. *J. Phys. Chem. B* **2008**, *112*, 5039–5046.

- (7) Kaminski, G. A.; Friesner, R. A.; Tirado-Rives, J.; Jorgensen, W. L. Evaluation and reparameterization of the OPLS-AA force field via comparison with accurate quantum chemical calculations on peptides. *J. Phys. Chem. B* **2001**, *105*, 6474–6487.
- (8) Jorgensen, W. L.; Chandrasekhar, J.; Madura, J. D.; Impey, R. W.; Klein, M. L. Comparison of simple potential functions for simulating liquid water. *J. Chem. Phys.* **1983**, *79*, 926–935.
- (9) Gronenborn, A. M.; Filpula, D. R.; Essig, N. Z.; Achari, A.; Whitlow, M.; Wingfield, P. T.; Clore, G. M. A novel, highly stable fold of the immunoglobulin binding domain of streptococcal protein G. *Science* **1991**, *253*, 657–661.
- (10) Darden, T.; York, D.; Pedersen, L. Particle mesh Ewald: An $N \log(N)$ method for Ewald sums in large systems. *J. Chem. Phys.* **1993**, *98*, 10089–10092.
- (11) Essmann, U.; Perera, L.; Berkowitz, M. L.; Darden, T.; Lee, H.; Pedersen, L. G. A smooth particle mesh Ewald method. *J. Chem. Phys.* **1995**, *103*, 8577–8593.
- (12) Evans, D. J.; Holian, B. L. The Nose-Hoover thermostat. *J. Chem. Phys.* **1985**, *83*, 4069–4074.
- (13) Parrinello, M.; Rahman, A. Polymorphic transitions in single crystals: A new molecular dynamics method. *J. Appl. Phys.* **1981**, *52*, 7182–7190.
- (14) Tribello, G. A.; Bonomi, M.; Branduardi, D.; Camilloni, C.; Bussi, G. PLUMED 2: New feathers for an old bird. *Comp. Phys. Comm.* **2014**, *185*, 604–613.
- (15) Laio, A.; Parrinello, M. Escaping free-energy minima. *Proc. Nat. Acad. Sci. USA* **2002**, *99*, 12562–12566.
- (16) Lesch, V.; Heuer, A.; Holm, C.; Smiatek, J. Solvent effects of 1-ethyl-3-methylimidazolium acetate: solvation and dynamic behavior of polar and apolar solutes. *Phys. Chem. Chem. Phys.* **2015**, *17*, 8480–8490.